LETTER

The study on a mixed-phase I–N-TiO$_2$ for the treatment of azithromycin wastewater under visible light

Xiaowei Qian · Ning Zhang · Mingxia Xu · Chao Chen

Introduction

Photocatalysis has attracted worldwide research interest for several decades because of its potential utilization of solar energy. It has been demonstrated that TiO$_2$ is one of the most significant inorganic photocatalytic materials [1, 2]. However, due to the large band gap of ~3.2 eV, TiO$_2$ can only be activated in UV region [3]. To enhance its light-absorbing properties and photocatalytic efficiency under visible light, many attempts have been carried out, such as selective ion doping [4–12], noble metal supporting [13, 14], and composite-type semiconductor preparation [15–18], etc. Among these attempts, TiO$_2$ materials modified with two types of non-metal ions have attracted great attention over recent years, owing to their enhanced photocatalytic activity, for instance, F–I, C–N, N–F, N–P, and B–N-codoped TiO$_2$ [19–24]. In addition, studies show that TiO$_2$ with mixed phases could enhance photocatalytic activity because of the more efficient electron–hole separation on the "hot spots" at the rutile-anatase interfaces [25, 26]. In contrast to the above-doped materials, the doping I and N in TiO$_2$ lattice for substituting the similar-radius Ti^{4+} and O^{2-}, respectively, has been much less explored [27]. Up to now, only one literature about N–I-TiO$_2$ has been found, which is synthesized by

hydrolysis method, and N–I-TiO$_2$ exists only in anatase phase [27]. In this work, using precipitation-grinding method and controlling the calcined temperature at 350 °C, we firstly synthesized a mixed-phase I–N-TiO$_2$ material. It could be expected that I–N-codoped TiO$_2$ with mixed phases may have a significant effect on further improving the photocatalytic activity of TiO$_2$ and inducing a remarkable visible-light activity.

Azithromycin, which played a major role in the clinical therapy of the infection when the SARS crisis broke, is a kind of macrolide antibiotics commonly used in clinic. While the Azithromycin pharmaceutical wastewater is considered as an important class of organic pollutants, because of its potential hazardous effects on human being and the aquatic ecosystem [28, 29]. Therefore, it is imperative to develop effective methods for treatment of APW. Recently, the application of TiO$_2$ in environmental purification appears to be very attractive, due to the environmentally friendly purification process. In this study, the mixed-phase I–N-TiO$_2$ was applied to treat APW. The result shows that the mixed-phase I–N-TiO$_2$ exhibits superior photocatalysis activity of APW under visible light.

Experimental

Sample preparation

All chemicals (Sinopharm Chemical Reagent Co., Ltd) are reagent grade and without further purification. The Azithromycin pharmaceutical wastewater solution was provided by the Jiangxi Baishen Pharmaceutical Co., Ltd.

Ti (OC$_4$H$_9$)$_4$ (8 ml) was dripped into 50 ml aqueous of HIO$_3$ (1.24 g) under vigorous stirring, which gave yellow-colored precipitate. The resulted mixture was aged for

X. Qian · N. Zhang (✉) · M. Xu · C. Chen (✉)
Department of Chemistry, Nanchang University,
Nanchang 330031, People's Republic of China
e-mail: nzhang.ncu@163.com

C. Chen
e-mail: chaochen@ncu.edu.cn

4 days at room temperature (25 °C), and then dried at 80 °C. To prepare a homogeneous sample, the dried precipitate with 0.21 g urea was mixed by milling in an agate mortar for 8 h with a rotating speed of 300 rpm. The final mixed-phase I–N-TiO$_2$ was obtained by calcination at 350 °C for 3 h. For comparison, the I-doped TiO$_2$ or N-doped TiO$_2$ was synthesized with the similar procedure but without urea or HIO$_3$ doping.

Characterization

The X-ray diffraction patterns were collected on a Bede XRD DI SYSTEM with Cu K$_\alpha$ as the incident radiation. The surface area, pore parameter, and average pore diameter were analyzed by N$_2$ physisorption at 77 K on Micromeritics ASAP 2020 system. Surface areas and pore size distributions were determined using BET ($P/P_0 = 0.05$–0.30) and BJH methods, respectively, both through Autosorb for Windows® software, version 3.03. Raman spectra were measured with NXR FT-RAMAN (Thermo Nicolet) Raman Spectrometer using a 1,064 nm laser at a power of 20–50 mW under backscattering conditions. UV–Vis reflectance spectra were obtained on the Shimadzu 2501PC UV–Vis spectrophotometer, using BaSO$_4$ as the background. X-ray photoelectron spectroscopy (XPS) measurements were performed on a PHI Quantum 2000 XPS system with a monochromatic Al K$_\alpha$ resource and a charge neutralizer.

Photocatalytic reaction

Photochemical experiments were conducted in a jacketed cylindrical glass reactor, the visible-light source was a 500 W halogen–tungsten lamp equipped with a 400-nm UV cutoff filter to effectively remove the UV portion, which was put 25 cm above the surface of the liquid in the reactor (the light intensity in the visible-light region at the surface of the liquid was about 32 mW/cm^2, and the effect of the UV portion of lamp light can be neglected). Oxygen was bubbled into the solution during the entire experiment at room temperature. Prior to illumination, the suspension was stirred in darkness for 30 min to achieve the adsorption–desorption equilibrium. For comparison, commercial P25 (Degussa P25, Degussa Chemical, Germany) was selected as a reference sample. The photocatalytic activity was identified by determining the Chemical Oxygen Demand (COD) of the reaction liquid using potassium dichromate method. COD removal rate (D %) was calculated by:

$$D\,(\%) = [(COD_0 - COD_t)\,/\,COD_0] \times 100$$

where COD$_0$ and COD$_t$ are the COD of initial and residual wastewater, respectively.

Results and discussion

Structural characteristics of samples

The crystalline structure, crystal size, and BET surface areas of all samples are listed in Table 1. It can be seen that all the doped samples exhibited larger surface area and smaller crystal size than the reference P25. The I–N-TiO$_2$, with the highest photoactivity (seen in the section of photocatalytic activity under visible light), shows modest surface area and crystal size, though both of them change somewhat with the adding of dopant iodine or nitrogen. XRD was used to determine the structures of the catalysts. The patterns of all samples (Fig. 1) reveal that the mono-doped samples display only anatase phase. However, the codoped TiO$_2$ exhibits predominantly anatase phase with a small amount of rutile phase (corresponding to the peak at $2\theta = 27.5$) [30, 31]. According to Hurum et al. [26], the co-existence of rutile and anatase is more important to the activity of the catalyst than the only presence of anatase. The presence of small rutile crystallites creates a structure, which results in rapid electron transfer from rutile to lower energy anatase lattice trapping sites under visible illumination, thus leading to a more stable charge separation. It is noteworthy that the anatase-to-rutile phase transformation temperature of I–N-TiO$_2$ is only 350 °C, which is much lower than that of pure TiO$_2$ ($\sim$700 °C). Due to the lattice distortion and bond weakening resulted from the introduction of I and N into TiO$_2$ lattice [32], the I–N codoping has an effect on decreasing the activation energy for the rutile formation [18], which facilitates the phase transformation.

Raman spectra analysis

The Raman spectra of all samples are shown in Fig. 2. I-TiO$_2$ and N-TiO$_2$ exhibit Raman bands at $\sim$149, 401, 518, and 640 cm^{-1}, which are assigned to E_g, B_{1g}, $A_{1g} + B_{1g}$, and E_g modes in anatase phase [33]. For I–N-TiO$_2$, the peak at 448 cm^{-1} belongs to E_g phonon mode of

Table 1 Physicochemical properties of the reference and prepared samples

Samples	Phase XRD	S_{BET} (m^2/g)	Pore size (nm)	Pore volume (cm^3/g)	Crystal size (nm)[a] XRD
P25	A + R[b]	48	21	0.25	30
N-TiO$_2$	A	176	39	0.24	15.1
I-TiO$_2$	A	169	72	0.34	7.2
I–N-TiO$_2$	A + R	107	64	0.23	10.2

[a] Obtained using Scherrer equation

[b] A and R denote anatase and rutile, respectively

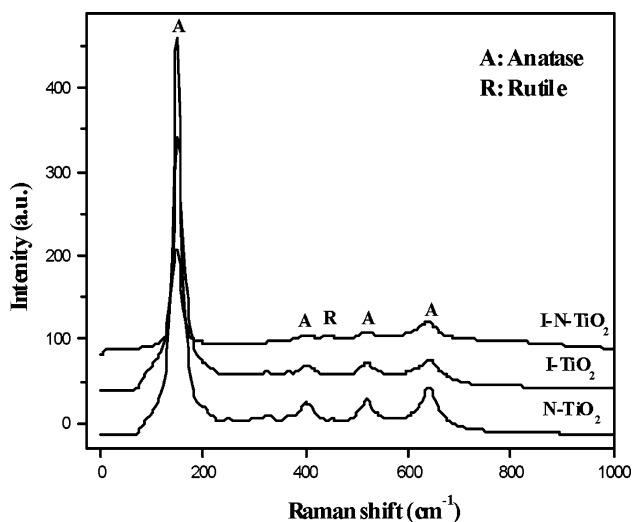Fig. 1 XRD patterns of N-TiO$_2$, I-TiO$_2$, and I–N-TiO$_2$

Fig. 2 Raman spectra of N-TiO$_2$, I-TiO$_2$ and I–N-TiO$_2$

Fig. 3 UV–Visible spectra of N-TiO$_2$, I-TiO$_2$, and I–N-TiO$_2$

rutile-type [34], and the other peaks are attributed to anatase phase. The results indicate that both anatase and rutile phase appear in the codoped TiO$_2$, which is in accordance with the XRD results.

UV–Vis diffuse reflectance spectra

The UV–Vis diffuse reflectance spectra of all the samples with different dopings are shown in Fig. 3. In comparison with pure TiO$_2$ ($E_g = 3.2$ eV, $\lambda_{max} < 387$ nm), photoabsorption of TiO$_2$ doped with N, I, and N–I all exhibit red shift (400 nm for N-TiO$_2$, 470 nm for I-TiO$_2$, and 570 nm for N–I-TiO$_2$), which is probably due to the formation of impurity energy level within the band gap [35]. Further inspection of the three doped TiO$_2$ reveals that the I–N-TiO$_2$ shows the strongest visible-light absorption and
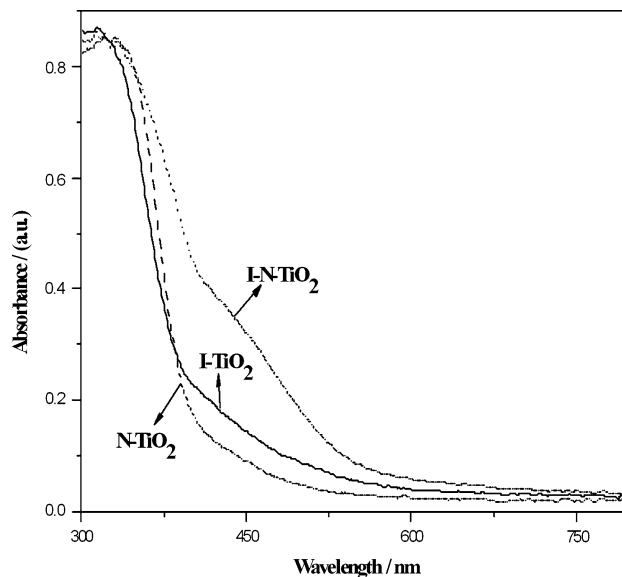
narrowest band gap (2.16 eV) than the other two. This suggests that I–N codoping resulted in a synergistic effect, which could significantly improve the visible-light absorption and reduce the band gap of TiO$_2$.

XPS analysis

XPS analyses were carried out to evaluate the electronic environment and valence state of the doped ions in TiO$_2$. The XPS spectrum of I$_{3d5}$ region presents three peaks at binding energies of 618.5, 624, and 629.2 eV (Fig. 4a). The peak corresponding to 629.2 eV is assigned to I^{5+} that substitutes Ti^{4+} in TiO$_2$ lattice, owing to their similar ionic radius [6]. The other two appeared at 618.5 and 624 eV should be attributed to I$^-$ and I^{7+}, respectively, due to the disproportionation of iodate ion. Figure 4b shows a major peak at 399.8 eV, which is typical for the surface adsorbed N-containing compounds (e.g. NH$_x$ and NO$_x$ adsorbed on the surface) [19, 31, 36]. The peak at 397.05 eV is assigned to nitrogen in the TiO$_2$ lattice as O–Ti–N, which is similar to previous studies [37]. Therefore, it is reasonable to be thought that both I and N have been doped into the bulk of TiO$_2$.

As shown in Fig. 5, the O$_{1s}$ peak of various samples has a similar binding energy. The main peak is at 529.7 eV and the shoulder peak at 531.7 eV, which could be attributed to the lattice oxygen and surface hydroxyl [32], respectively. It is interesting to note that the total amount of surface hydroxyl oxygen of codoped TiO$_2$ is larger than that of those mono-doped TiO$_2$ (Fig. 5d). The surface hydroxyl groups can not only act as the active adsorption sites for the molecular oxygen and organic compound, but also block the recombination of electron–hole pairs and capture

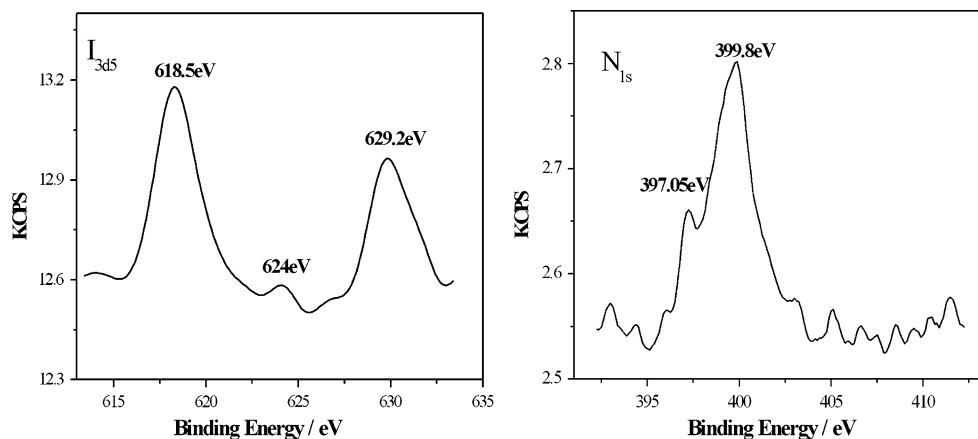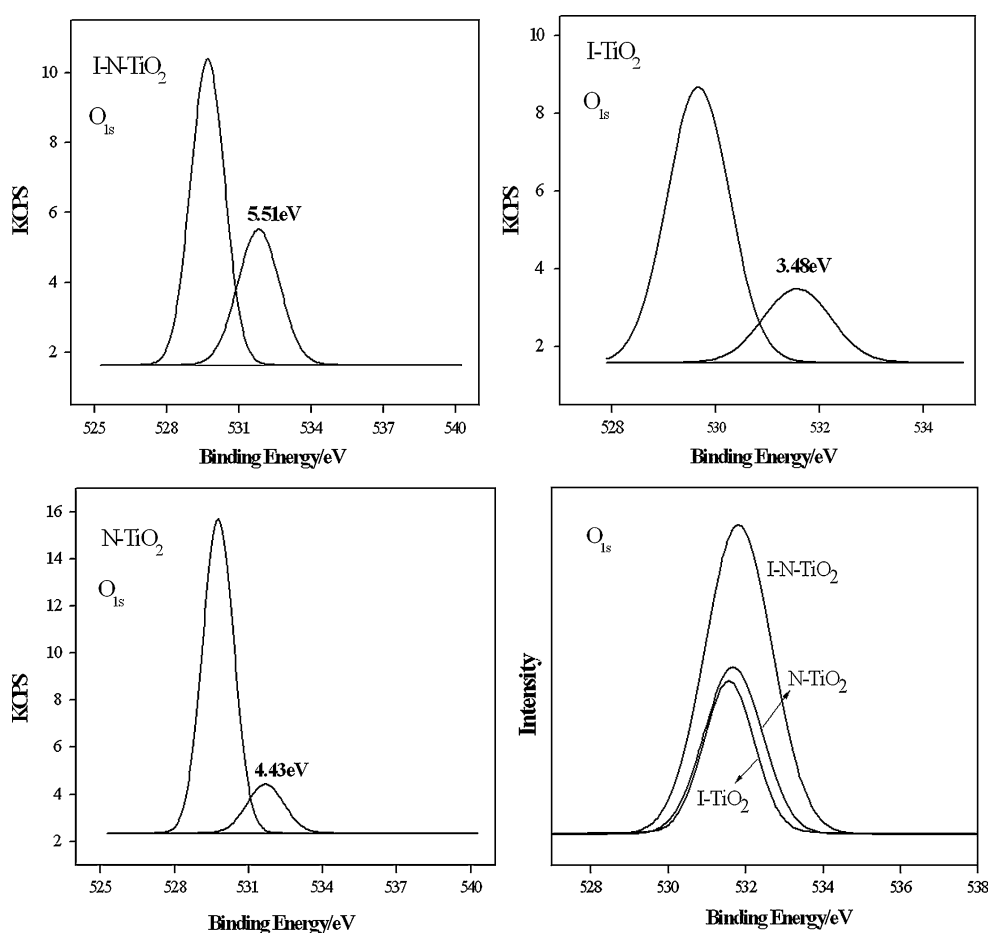**Fig. 4 a** I_{3d5} XPS spectra of I–N-TiO$_2$, **b** N$_{1s}$ XPS spectra of I–N-TiO$_2$

Fig. 5 O$_{1s}$ XPS spectra of **a** I–N-TiO$_2$, **b** I-TiO$_2$, **c** N-TiO$_2$, and **d** An expanded view of O$_{1s}$ XPS spectra of the surface hydroxyl peak

photogenerated holes to produce hydroxyl radical (•OH). As it is known, hydroxyl radical is recognized as an important factor affecting the photocatalytic activity and correlated well with the photocatalytic activity of catalyst [38]. It is important for both the photocatalytic oxidation activity and to mineralize organic pollutants [2, 39, 40]. Additionally, a small amount of C element was also detected in the sample of I–N-TiO$_2$ (283.3, 284.5, and 287.1 eV, Fig. S1), which was

ascribed to the adventitious hydrocarbon from the XPS instrument itself, the residual carbon from precursor solution and adventitious element carbon [6].

Photocatalytic activity under visible light

As illustrated in Fig. 6, after a 12-h reaction under visible light, the commercial P25 was nearly inactive for the
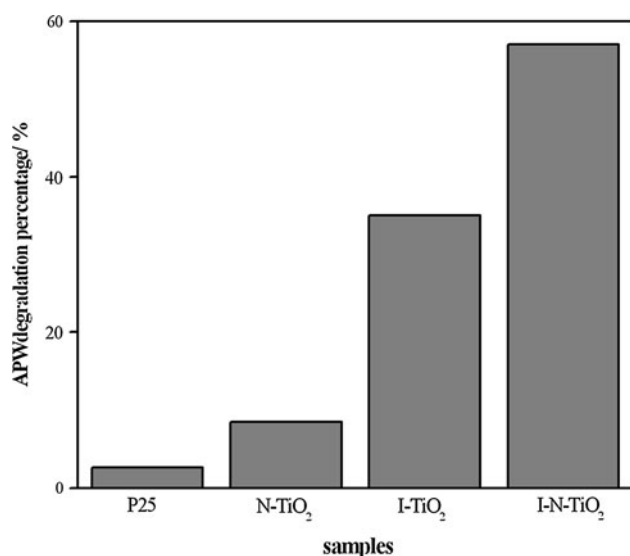
Fig. 6 Effect of type of samples on APW degradation percentage after a 12-h reaction

photodegradation of APW, and I–N-TiO$_2$ demonstrated the best photocatalytic activity (57% degradation of APW) as compared with I-TiO$_2$ (35%) and N-TiO$_2$ (8%). Based on the above characterization results and discussions, we proposed that its superior activity could be ascribed to the mixed-phase structure, the synergetic actions of the iodine and nitrogen, and the relatively more surface hydroxyl groups. According to our knowledge, this is the first time that the non-metal-doped TiO$_2$ materials have been applied in the photocatalytic treatment of Pharmaceutical wastewater.

Conclusions

In summary, a new I–N-TiO$_2$ with mixed phases was obtained by precipitation-grinding method. As compared with N-TiO$_2$ or I-TiO$_2$ catalysts, the mixed-phase I–N-TiO$_2$ exhibits a higher photocatalytic activity under visible irradiation during the photocatalytic treatment of APW. The higher activity of the codoped TiO$_2$ may be ascribed to the mixed-phase structure, the synergetic interactions of the iodine and nitrogen, and the relatively more surface hydroxyl groups. Further studies will be focused on the optimization of the preparation conditions of photocatalysts and the photocatalytic treatment conditions.

References

1. Fujishima A, Honda K (1972) Nature 238:37
2. Hoffmann MR, Martin ST, Choi WY, Bahnemann DW (1995) Chem Rev 95:69
3. Chio W, Termin A, Hoffman MR (1994) J Phys Chem 98:13669
4. Chen XF, Wang WC, Hou YD, Huang JH, Wu L, Fu XZ (2008) J Catal 255:59
5. Yu CL, Zhou WQ, Yang K, Rong G (2010) J Mater Sci 45:5756. doi:10.1007/s10853-010-4646-6
6. Hong XT, Wang ZP, Cai WM, Zhang J, Yang YZ (2005) Chem. Mater 17:1548
7. Randeniya LK, Murphy AB, Plumb IC (2008) J Mater Sci 43:1389. doi:10.1007/s10853-007-2309-z
8. Masanori H, Yoshiko I (2009) J Mater Sci 44:6135. doi:10.1007/s10853-009-3848-2
9. Chen C, Long MC, Zeng H, Cai WM, Zhou BX, Zhang JY, Wu YH, Ding DX, Wu DY (2009) J Mol Catal A 314:35
10. Shet S, Ahn KS, Wang HL (2010) J Mater Sci 45:5218. doi:10.1007/s10853-010-4561-x
11. Songara S, Patra MK, Manoth M, Saini L, Gupta V, Gowd GS, Vadera SR, Kumar N (2010) J Photochem Photobiol A 209:68
12. Wei HY, Wu YS, Lun N, Zhao F (2004) J Mater Sci 39:1305. doi:10.1023/B:JMSC.0000013889.63705.f3
13. Rosseler O, Shankar MV, Du MK-L, Schmidlin L, Keller N, Keller V (2010) J Catal 269:179
14. Paramasivam I, Macak JM, Schmuki P (2008) Electrochem Commun 10:71
15. Kim HJ, Lee SH, Han Y, Park JK (2006) J Mater Sci 41:6150. doi:10.1007/s10853-006-0574-x
16. Wang C, Xu BQ, Wang XM, Zhao JC (2005) J Solid State Chem 178:3500
17. Chen JY, Qian YX, Wei XZ (2010) J Mater Sci 45:6018. doi:10.1007/s10853-010-4685-z
18. Irie H, Watanabe Y, Hashimoto K (2003) J Phys Chem B 107:5483
19. Li D, Ohashi N, Hishita S, Kolodiazhnyi T, Haneda H (2005) J Solid State Chem 178:3293
20. Chen C, Cai WM, Long MC, Zhang JY, Zhou BX, Wu YH, Wu DY (2010) J Hazard Mater 178:560
21. Di Valentin C, Finazzi E, Pacchioni G, Selloni A, Livraghi S, Czoska AM, Paganini MC, Giamello E (2008) Chem Mater 20:3706
22. Long R, English NJ (2010) J Phys Chem C114:11984
23. Shao GS, Ma TY, Zhang XJ (2009) J Mater Sci 44:6754. doi:10.1007/s10853-009-3628-z
24. Suil I, Alexander O, Regina B, Felipe G, Sergio PJ, Mintcho ST, Dominic SW, Richard ML (2007) J Am Chem Soc 129:13790
25. Bacsa RR, Kiwi J (1998) Appl Catal B 16:19
26. Hurum DC, Agrios AG, Gray KA, Rajh T, Thurnauer MC (2003) J Phys Chem B 107:4545
27. Zhou L, Deng J, Zhao YB, Liu WB, An L, Chen F (2009) Mater Chem Phys 117:522
28. Calza P, Massolino C, Monaco G, Medana C, Baiocchi C (2008) J Pharm Biomed 48:315
29. Hapeshi E, Achilleos A, Vasquez ML, Michael C, Xekoulotakis NP, Mantzavinos D, Kassinos D (2010) Water Res 44:1737
30. Kang XW, Chen SW (2010) J Mater Sci 45:2696. doi:10.1007/s10853-010-4254-5
31. Su WY, Zhang YF, Li ZH, Wu L, Wang XX, Li JQ, Fu XZ (2008) Langmuir 24:3422
32. Tojo S, Tachikawa T, Fujitsuka M, Majima T (2008) J Phys Chem C 112:14948
33. Ohsaka T, Izumi F, Fujiki Y (1978) J Raman Spectrosc 7:321
34. Chaves A, Katiyar RS, Porto SPS (1974) Phys Rev B10:3522

35. Long MC, Cai WM, Wang ZP, Liu GZ (2006) Chem Phys Lett 420:71
36. Asahi R, Morikawa T, Ohwaki T, Aoki K, Tag Y (2001) Science 293:269
37. Parida KM, Naik B (2009) J Colloid Interface Sci 333:269
38. Xiao Q, Ouyang LL (2009) Chem Eng J 148:248
39. Ihara T, Miyoshi M, Iriyama Y, Matsumoto O, Sugilara S (2003) Appl Catal B Environ 42:403
40. Litter MI (1999) Appl Catal B Environ 23:89